PRAMANA — journal of physics

Vol. 81, No. 6
December 2013
pp. 1021–1035

Phonon dispersions in graphene sheet and single-walled carbon nanotubes

DINESH KUMAR[1,*], VEENA VERMA[2], H S BHATTI[1] and KEYA DHARAMVIR[3]

[1]Department of Physics, Punjabi University, Patiala 147 002, India
[2]Department of Physics, Govt. Shivalik College, Naya Nangal District, Ropar 140 126, India
[3]Centre for Advance Study in Physics, Panjab University, Chandigarh 160 014, India
*Corresponding author. E-mail: dineshk_2@yahoo.co.in

MS received 31 March 2013; revised 31 August 2013; accepted 11 September 2013
DOI: 10.1007/s12043-013-0625-1; ***e*Publication:** 26 November 2013

Abstract. In the present research paper, phonons in graphene sheet have been calculated by constructing a dynamical matrix using the force constants derived from the second-generation reactive empirical bond order potential by Brenner and co-workers. Our results are comparable to inelastic X-ray scattering as well as first principle calculations. At Γ point, for graphene, the optical modes (degenerate) lie near 1685 cm^{-1}. The frequency regimes are easily distinguishable. The low-frequency ($\omega \to 0$) modes are derived from acoustic branches of the sheet. The radial modes can be identified with $\omega \to 584$ cm^{-1}. High-frequency regime is above 1200 cm^{-1} (i.e. ZO mode) and consists of TO and LO modes. The phonons in a nanotube can be derived from zone folding method using phonons of a single layer of the hexagonal sheet. The present work aims to explore the agreement between theory and experiment. A better knowledge of the phonon dispersion of graphene is highly desirable to model and understand the properties of carbon nanotubes. The development and production of carbon nanotubes (CNTs) for possible applications need reliable and quick analytical characterization. Our results may serve as an accurate tool for the spectroscopic determination of the tube radii and chiralities.

Keywords. Graphene; carbon nanotubes; force constants and dynamical matrix; phonon dispersions; vibrational density of states; specific heat; radial breathing mode.

PACS No. 63.22.Rc

1. Introduction

A phonon is a quantized mode of vibration occurring in a rigid crystal lattice, such as the atomic lattice of a solid. The study of phonons is important in solid-state physics, because phonons play a major role in many of the physical properties of solids, including a material's thermal and electrical conductivities. In particular, the properties of

long-wavelength phonons give rise to sound in solids, hence the name phonon comes from the Greek phonē meaning voice. Phonons are a quantum mechanical version of a special type of vibrational motion, known as normal modes in classical mechanics, in which each part of a lattice oscillates with the same frequency. These normal modes are important because, any arbitrary vibrational motion of a lattice can be considered as a superposition of normal modes with various frequencies; in this sense, the normal modes are the elementary vibrations of the lattice. Although normal modes are wave-like in classical mechanics, they acquire particle-like properties when the lattice is analysed using quantum mechanics. They are then known as phonons. A number of models [1–8] have been proposed to calculate the phonon dispersion in bulk graphite. Most improved ones [5,6] involve up to 20 parameters. Details of first principle calculations of optical phonon frequencies for graphite are given in [9,10] which shows qualitative disagreement with the models [1,8], that includes the central and angular atomic forces between the first and the second neighbours in the graphite lattice. The passage in the lattice dynamics from graphite to its single layer, i.e. graphene and then to nanotubes was examined in the *ab initio* calculation [11,12], in [13] using the model [1], and in [14] up to the fourth neighbour with 12 force constants. Numerical calculations, based on Huckel's theory [15] and in terms of the electron energy, were performed in [16]. The first-principle calculations [17] of dynamical properties for graphite and graphene show that distinctions between the phonon frequencies in graphene and graphite are negligible in comparison with the experimental errors for that frequencies in graphite. For the highest frequencies, this can be intuitively expected because interactions between the adjacent layers in graphite are weak. Our aim here is to find an analytical description of the phonon dispersion in graphene. This can be done within the framework of the model potential, i.e. second generation reactive empirical bond order potential by Brenner and co-workers [18] for the honeycomb graphene lattice with interactions only between the first and second nearest neighbours, but the constraints imposed by the lattice symmetry should be taken to account.

2. Acoustic and optical phonons

In solids with more than one atom in the smallest unit cell, there are two types of phonons: acoustic phonons and optical phonons. Acoustic phonons have frequencies that become smaller at long wavelengths, and correspond to sound waves in the lattice. Longitudinal and transverse acoustic phonons are often abbreviated as LA and TA phonons, respectively. In crystals with more than one atom in the smallest unit cell, optical phonons also arise, which always have some minimum non-zero frequency of vibration, even when their wavelength is large. They are called optical because in ionic crystals (like sodium chloride) they are excited very easily by light (in fact, infrared radiation). This is because they correspond to a mode of vibration where positive and negative ions, at adjacent lattice sites, swing against each other, creating a time-varying electrical dipole moment. Optical phonons that interact in this way with light are called infrared active. Optical phonons which are Raman active can also interact indirectly with light, through Raman scattering. Optical phonons are often abbreviated as LO and TO phonons, for the longitudinal and transverse varieties respectively.

3. Method of calculation

We know that the quantities $D_{\alpha i}^{\beta j}(\vec{q})$ form the dynamical matrix [19]. The system of equations is a linear homogeneous system of order $3r$ in a three-dimensional system, where r is the number of atoms per unit cell.

For 3D system [20], we have $3r$ different solutions. For non-trivial solutions, we should have

$$\mathrm{Det}\{D_{\alpha i}^{\beta j}(\vec{q}) - \omega^2 \delta_{\alpha\beta}\delta_{ij}\} = 0, \tag{1}$$

where

$$D_{\alpha i}^{\beta j}(\vec{q}) = \frac{1}{\sqrt{M_\alpha M_\beta}} \sum_m \phi_{0\alpha i}^{m\beta j} \exp(i\vec{q}\cdot\vec{r}). \tag{2}$$

Here $\vec{r}_m$ is the position vector of the mth cell which contains two atoms. Here masses M_α and M_β are masses of αth and βth atoms respectively. $\phi_{0\alpha i}^{m\beta j}$ are the force constants which are to be calculated using second-generation reactive empirical bond order potential.

3.1 *Model potential*

3.1.1 *A second-generation reactive empirical bond order (REBO) potential.* In this work we have used an improved 'second-generation' form of the potential [21–23] and the details of this potential energy expressions are given below. The energy of the system is a sum of the energy of each C–C bond composed of a repulsive part and an attractive part. In this second-generation potential [18], commonly known as a reactive empirical bond order (REBO) potential, the forms

$$V_{\mathrm{R}}(r) = f_{\mathrm{c}}(r)\left(1 + \frac{Q}{r}\right) A\mathrm{e}^{-\alpha r} \tag{3}$$

and

$$V_{\mathrm{A}}(r) = f_{\mathrm{c}}(r) \sum_{n=1,3} B_n \mathrm{e}^{-\beta_n r} \tag{4}$$

are used for repulsive and attractive pair terms respectively. The subscript n refers to the sum in eq. (4) and r is the scalar distance between atoms. The screened Coulomb function used for the repulsive pair interaction goes to infinity as interatomic distances approach zero. The function $f_{\mathrm{c}}(r)$ limits the range of the covalent interactions and it assumes a value of one for nearest neighbours and zero for interatomic distances more than 2.1, and expression for $f_{\mathrm{c}}(r)$ is given as

$$f_{\mathrm{c}}(r) = \begin{cases} 1, & r < (R - D), \\ \dfrac{1}{2} - \dfrac{1}{2}\sin\left[\dfrac{1}{2}\dfrac{\pi(r-R)}{D}\right], & (R-D) < r < (R+D), \\ 0, & r > (R+D). \end{cases}$$

The second-generation REBO potential takes into account the stretching and bending of C–C bonds in graphene sheet as well as CNTs. The force constants $\phi_{0\alpha i}^{m\beta j}$ are the second derivative of the energy with respect to stretching and bond bending as shown in figure 1.

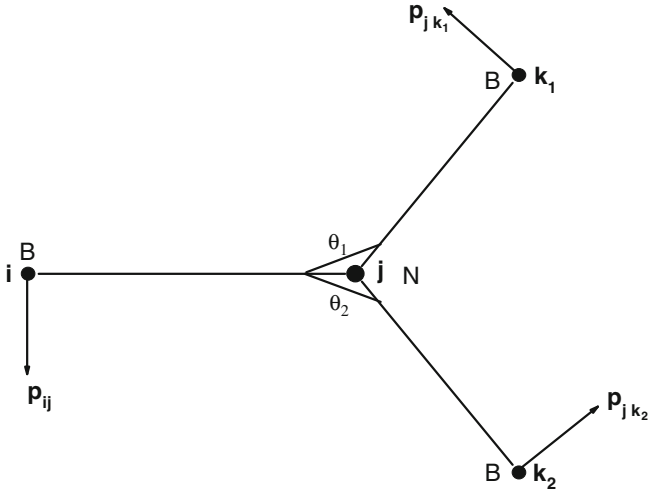

Figure 1. Bond angles.

A slight change in position of the atom i, k_1 or k_2 can change the bonding angle which in turn changes the bonding strength.

3.2 *Description of unit cell and lattice vectors*

We consider a two-dimensional sheet of graphene. A part of the generated sheet used for the calculations is shown in figure 2. The figure shows the hexagonal unit cells as well as the parallelepipeds defining the crystal lattice, in which the basis consists of two atoms. The lattice vectors are shown with bold arrows. The atomic sites are marked with integers 0, 1, 2 etc. and the cells are marked with (**0**), (**1**), (**2**), etc. We shall need only these six cells for our calculations as all the second neighbours of atoms belonging to the 0th cell

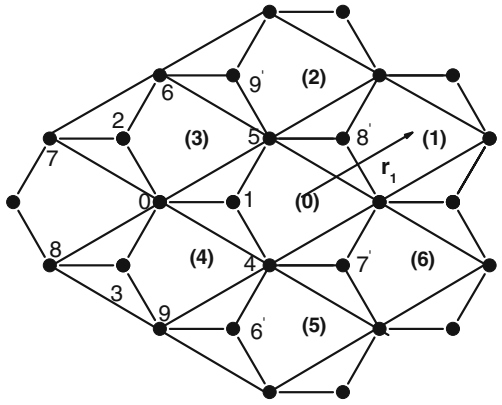

Figure 2. Unit cells in a hexagonal lattice containing C–C atoms.

are contained within these. The lattice vector of cell (1) (connecting the centre of cell (0) to the centre of cell (1)) is shown as an arrow. All the relevant lattice vectors thus obtained are listed below:

$$\vec{r}_1 = \left(\frac{3b}{2}\right)\hat{x} + \left(\frac{\sqrt{3}b}{2}\right)\hat{y},$$

$$\vec{r}_2 = 0\hat{x} + \sqrt{3}b\hat{y},$$

$$\vec{r}_3 = \left(\frac{-3b}{2}\right)\hat{x} + \left(\frac{\sqrt{3}b}{2}\right)\hat{y},$$

$$\vec{r}_4 = -\left(\frac{3b}{2}\right)\hat{x} - \left(\frac{\sqrt{3}b}{2}\right)\hat{y} = -\vec{r}_1,$$

$$\vec{r}_5 = 0\hat{x} - \sqrt{3}b\hat{y} = -\vec{r}_2,$$

$$\vec{r}_6 = \left(\frac{3b}{2}\right)\hat{x} - \left(\frac{\sqrt{3}b}{2}\right)\hat{y} = -\vec{r}_3.$$

We shall also need to index the atoms differently in order to conform to the notation in $\phi_{0\alpha i}^{m\beta j}$. So the atom with index 0 shown in the diagram, which is of type 1 belonging to the (0)th cell, must be identified as the 01th atom. Similarly, the atom numbered 1 in the diagram is the 02th atom in this notation. The conversion between these two types of notations is given in Appendix I and is handy in the calculations.

3.3 *Construction of a dynamical matrix for graphene sheet*

We numerically evaluate the second derivative involving atoms in the central cell going up to fourth neighbour. In order to evaluate the force constants we use the numerical differentiation procedure. We generate a sheet of 31 atoms and obtain the values of elements of dynamical matrix. We do this by evaluating the various energies of this system when either one or two of the atoms are displaced by a small amount Δ, e.g. in expressions given in Appendix II, s_{ni} denotes the displacement of the nth atom in figure 2 in the ith direction where $i = 1$ and 2 mean x and y. Using second-generation reactive empirical bond order potential, the calculated values of various force constants are given in Appendix III.

If $j \neq 3$, then $\phi_{013}^{n\alpha j} = 0$. For this reason, the dynamical matrix has a box diagonal form, with the elements containing the third dimension separated out. For this reason we solve only the 6×6 matrix corresponding to x–y–z displacements in the sheet. This is described below. Using the force constants obtained, we find the elements of the dynamical matrix using eq. (2). The first element $D(1, 1)$ is calculated as below:

$$D_{11}^{11} = \frac{1}{M_1}[\phi_{011}^{022} + \textstyle\sum_K \phi_{011}^{J22} \exp i(\vec{q}\,\vec{r}_i)]$$

$$= D_{11}^{11} = \frac{1}{M_1}[151.31817 + 2 * 7.56922 * \cos(2yy) - 2 * 1.498 * \cos(xx) * \cos(yy)],$$

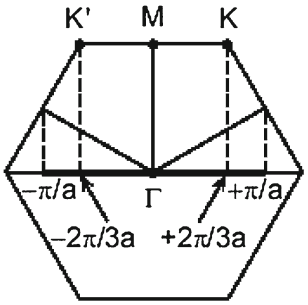

Figure 3. Symmetry points in a single hexagon.

where $xx = 3b_0q_x/2$ and $yy = \sqrt{3}b_0q_x/2$. Proceeding similarly, we get all the 6×6 elements of the dynamical matrix. So eq. (1) now becomes

$$\begin{vmatrix} D_{11}^{11} - \omega^2 & D_{11}^{12} & D_{11}^{21} & D_{11}^{22} \\ D_{12}^{11} & D_{12}^{12} - \omega^2 & D_{12}^{21} & D_{12}^{22} \\ D_{21}^{11^*} & D_{21}^{12} & D_{22}^{21} - \omega^2 & D_{21}^{22} \\ D_{22}^{11^*} & D_{22}^{12^*} & D_{22}^{21} & D_{22}^{22} - \omega^2 \end{vmatrix} = 0.$$

We diagonalize the matrix using one of the standard available programs. Since the number of dispersion relations in a 3D lattice is given by $3N$ (N is the number of atoms in a unit cell), there being two atoms per unit cell in a graphene sheet, there are six phonon dispersion curves in each symmetry direction. The symmetry points are shown in figure 3. The phonon dispersion curves are shown in figure 4. Note that in spite of the system being two-dimensional, the displacements are allowed in all three directions (including the

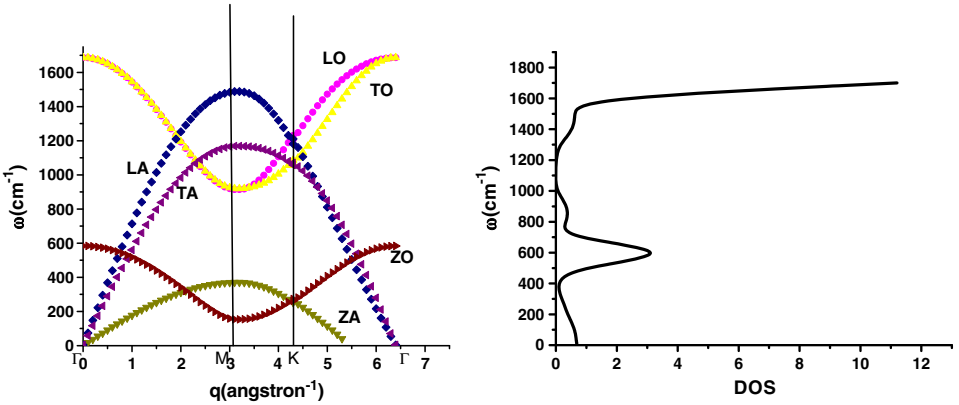

Figure 4. Phonon dispersion of graphene and DOS graphene.

Table 1. Range of frequency of all branches of graphene.

Branch	$\omega_{max}(cm^{-1})$ Graphene	$\omega_{min}(cm^{-1})$ Graphene	
TO	1685 (1581)[a]	1068	
LO	1685, (1583)[b], (1582)[a]	1265	
LA	1210	0–919	Zero at Γ pt., (0)[a]
TA	1210	0–914	Zero at Γ pt.
ZO	584	370	
ZA	370	0–153	Zero at Γ pt.

[a]Theoretical [9].
[b]Experimental [9].

z-direction perpendicular to the plane). Hence there are $3N$ branches and not $2N$. Range of frequency of all branches of graphene is shown in table 1.

The phonons in a nanotube can be derived by zone folding method using phonons of a single layer of the hexagonal sheet.

4. Zone folding method

To calculate the phonon dispersion relation (PDR) and vibrational density of states (VDOS) of CNTs, we adopt the zone folding method which is used for calculating electronic band structure as well as phonons in CNTs. Since the CNT is infinite only in one dimension (say y direction), only q_y has quasicontinuous nature. In the x-direction, the tube is obtained by folding the rectangular sheet along the x-direction. For calculating phonons, the periodicity along x-direction is taken to be the width of the sheet (radius of the nanotube). Therefore, q_x is restricted to only certain values depending on the finite width. Each line on the phonon dispersion curve represents one of these allowed q_x values. We find that there is no real band gap when the sheet is folded into CNT. We calculate the PDR and VDOS of the (4,4) and (10,10) CNTs. The results are shown in figure 5. Our results are also comparable to Maultzsch *et al* [9] who measured the dispersion of the graphite optical phonons in the in-plane Brillouin zone by inelastic X-ray scattering as well as first principle calculations.

We also calculate the specific heat of (4,4) and (10,10) CNT and this is depicted in figure 6. As expected, the specific heat of (10,10) CNT approaches a constant value at the high temperature limit and a linear T dependence at low temperature.

5. Radial breathing modes in carbon nanotube

For interpreting and understanding theoretical models for studying any system, pressure and temperature dependence of structural and dynamical properties are very useful. The

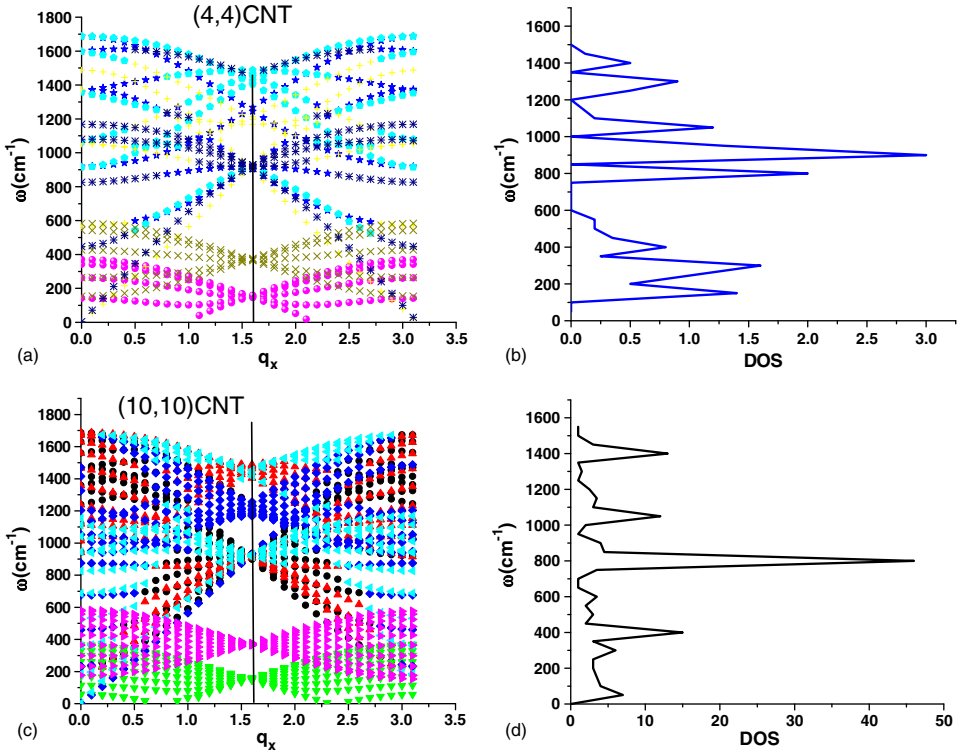

Figure 5. PDR (**a**, **c**) and DOS (**b**, **d**) for (4,4) and (10,10) CNTs.

variation of temperature and pressure results in changes in the ordered environment of the system which can undergo phase transitions. To study the thermal properties of single-walled CNT (SWCNT) system, lattice heat capacity is an important parameter. The

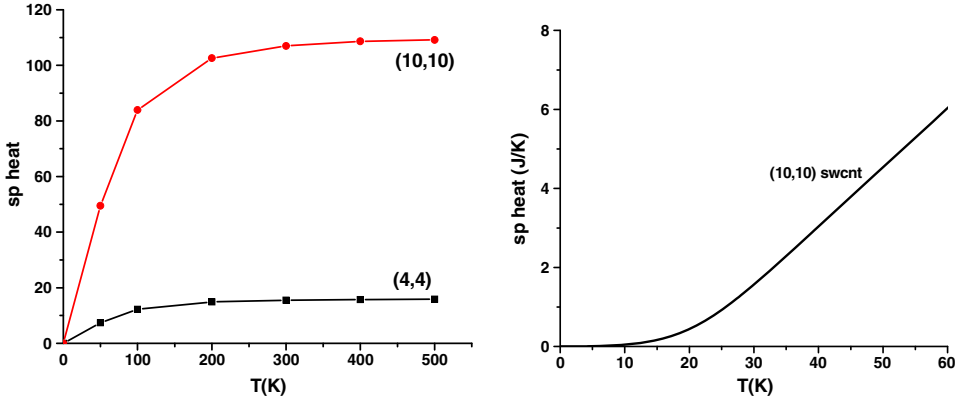

Figure 6. Specific heat of CNT (high and low temperature region).

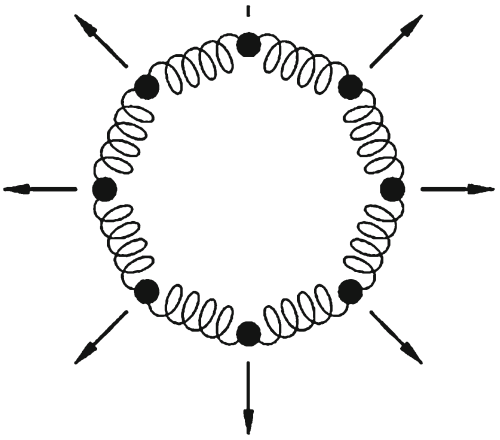

Figure 7. Radial breathing mode.

most important low-frequency Raman active mode of nanotubes is called radial breathing mode (RBM). When all the atoms move in a phase perpendicular to the tube axis, by changing the radius of the tube, one gets the RBM. It involves the collective movement of atoms towards and away from the central axis of the SWCNT. The radial breathing mode emerges from the periodicity of the two-dimensional hexagonal lattice, when it is wrapped to form a CNT. Therefore the frequency of this mode is directly influenced by the perimeter of the tube as shown in figure 7. We have calculated the radial breathing mode for a family of zig-zag and armchair CNTs.

We have changed the radius of a particular tube by a very small amount and calculated the force constants for each tube and hence the RBM. As shown in table 2, and figure 8, RBM approaches the sheet value as the radius of the tube is increased which matches the ZO values in the dispersion curve.

Table 2. Phonon calculation for CNT.

RBM (CNT)	Wave number (cm^{-1})
(5,5)	2134
(10,10)	1511
(15,15)	1206
(20,20)	1017
(25,25)	881
(9,0)	345
(12,0)	267
(15,0)	212.6
(18,0)	178.9
(21,0)	154.7

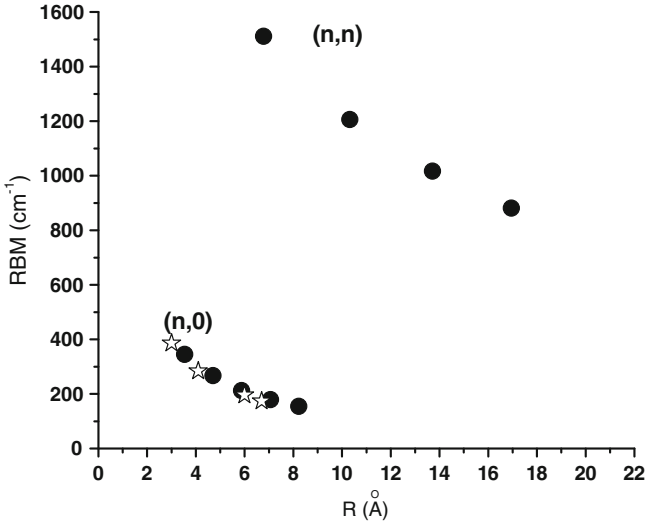

Figure 8. Radial breathing mode of (n,n) and (n,0) CNTs (solid circles) and from experiment (stars) [24].

The variation of RBM with the radius of the tubes is shown in figure 8 for CNTs. Our results match well with experimental and theoretical values reported by others for zig-zag CNTs [25–27]. Though RBM varies inversely with radius for both types of tubes, there is a clear distinction between armchair and zig-zag tubes. Our results may serve as an accurate tool for the spectroscopic determination of tube radii and chiralities.

6. Summary and conclusions

In this work, we have calculated the phonons in graphene sheet and radial breathing modes of CNTs. Our dispersion relations match qualitatively well with [15]. At Γ point the optical modes (degenerate) lie near 1685 cm^{-1} for graphene which is a little higher than the reference calculations. The acoustic modes split at M and K points respectively in their work, the former splitting being larger than the latter. In our work, the latter splitting vanishes at the zone boundary. The range of optical modes also matches in the two works. The phonons in a nanotube can be derived by zone folding method using phonons of a single layer of the hexagonal sheet. Our results match well with experimental and theoretical values reported by others for zig-zag CNTs [25–27] but our values for armchair CNTs are higher than zig-zag tubes. Though RBM varies inversely with radius for both types of tubes, there is a clear distinction between armchair and zig-zag tubes. Our results may serve as an accurate tool for the spectroscopic determination of tube radii and chiralities.

Appendix I

Table A. Indices of the site of some of atoms

Index for atom	Index for the hexagon cell	Index for the type of atom
0	0	1
1	0	2
2	3	2
3	4	2
4	6	1
5	1	1
6	2	1
7	3	1
8	4	1
9	5	1
6′	5	2
7′	6	2
8′	1	2
9′	2	2

Appendix II. Numerical differentiation procedure for evaluating force constants

$$\begin{aligned}\frac{\partial^2\phi}{\partial s_{01}\partial s_{11}} &= \frac{\partial}{\partial_{01}}\frac{\partial\phi}{\partial s_{11}}\\ &= \frac{1}{2\Delta}\left[\left(\frac{\partial\phi}{\partial s_{11}}\right)_{x0=\Delta x} - \left(\frac{\partial\phi}{\partial s_{01}}\right)_{x0=-\Delta}\right]\\ &= \frac{1}{4\Delta^2}\left[(\phi(x_1=\Delta)-\phi(x_1=-\Delta))_{x0=\Delta}\right.\\ &\qquad \left. -\,(\phi(x_1=\Delta)-\phi(x_1=-\Delta))_{x0=-\Delta}\right]\\ &= \frac{1}{4\Delta^2}\left[\phi(x_0=\Delta, x_1=\Delta)-\phi(x_0=\Delta, x_1=-\Delta)\right.\\ &\qquad \left. -\,\phi(x_0=-\Delta, x_1=\Delta)+\phi(x_0=-\Delta, x_1=-\Delta)\right]\\ &= \frac{1}{4\Delta^2}\left[2\phi(x_0=\Delta, x_1=\Delta)-\phi(x_0=\Delta, x_1=-\Delta)\right.\\ &\qquad \left. -\,\phi(x_0=-\Delta, x_1=\Delta)\right], \qquad (5)\end{aligned}$$

$$\frac{\partial^2\phi}{\partial s_{01}\partial s_{12}} = 0 = \frac{\partial^2\phi}{\delta s_{02}\partial s_{11}}, \qquad (6)$$

$$\frac{\partial^2\phi}{\partial s_{02}\partial s_{12}} = \frac{1}{2\Delta^2}\left[\phi(y_0=\Delta, y_1=\Delta)-\phi(y_0=\Delta, y_1=-\Delta)\right], \qquad (7)$$

$$\frac{\partial^2\phi}{\partial s_{01}^2} = \frac{1}{\Delta^2}\left[\phi(x_0 = \Delta) + \phi(x_0 = -\Delta) - 2\phi_0\right], \tag{8}$$

$$\frac{\partial^2\phi}{\partial s_{02}^2} = \frac{2}{\Delta^2}\left[\phi(y_0 = -\Delta) - \phi_0\right]. \tag{9}$$

There are two non-vanishing terms only. Other terms are zero. We can find derivatives between 0 and 2 and 0 and 3 by the transformation of x and y as shown below. Choosing the primed coordinate system, x' from atom 0 to atom 2 and y' normal to it, we obtain

$$\begin{vmatrix} x' \\ y' \end{vmatrix} = \begin{vmatrix} \cos 120^\circ & -\sin 120^\circ \\ \sin 120^\circ & \cos 120^\circ \end{vmatrix} \begin{vmatrix} x \\ y \end{vmatrix},$$

where

$$x' = \frac{x}{2} - \frac{\sqrt{3}}{2}y, \tag{10}$$

$$y' = \frac{\sqrt{3}}{2}x - \frac{y}{2}, \tag{11}$$

$$\frac{\partial^2\phi}{\partial s_{01}\partial s_{11}} = \frac{\partial^2\phi}{\partial s_{01'}\partial s_{11'}}, \tag{12}$$

$$\begin{aligned}\frac{\partial\phi}{\partial s_{21}} &= \frac{\partial\phi}{\partial s_{21'}}\frac{\partial s_{21'}}{\partial s_{21}} + \frac{\partial\phi}{\partial s_{22'}}\frac{\partial s_{22'}}{\partial s_{22}} \\ &= -\frac{1}{2}\frac{\partial\phi}{\partial s_{21'}} - \frac{1}{2}\frac{\partial\phi}{\partial s_{22'}},\end{aligned} \tag{13}$$

$$\begin{aligned}\frac{\partial^2\phi}{\partial s_{01}\partial s_{21}} &= -\frac{1}{2}\frac{\partial}{\partial s_{01}}\frac{\partial\phi}{\partial s_{21'}} - \frac{1}{2}\frac{\partial}{\partial s_{01}}\frac{\partial\phi}{\partial s_{22'}} \\ &= -\frac{1}{2}\frac{\partial}{\partial s_{01'}}\frac{\partial\phi}{\partial s_{21'}}\left(\frac{\partial s_{01}}{\partial s_{01}}\right) - \frac{1}{2}\frac{\partial}{\partial s_{02'}}\frac{\partial\phi}{\partial s_{21'}}\left(\frac{\partial s_{02'}}{\partial s_{01}}\right) \\ &\quad -\frac{1}{2}\frac{\partial}{\partial s_{01'}}\frac{\partial\phi}{\partial s_{22'}}\left(\frac{\partial s_{01'}}{\partial s_{01}}\right) - \frac{1}{2}\frac{\partial}{\partial s_{02'}}\frac{\partial\phi}{\partial s_{22'}}\left(\frac{\partial s_{02'}}{\partial s_{01}}\right) \\ &\quad -\frac{1}{4}\frac{\partial^2\phi}{\partial s_{01'}\partial s_{21'}}\frac{\sqrt{3}}{4}\frac{\partial^2\phi}{\partial s_{02'}\partial s_{22'}} \\ &= \frac{1}{4}\frac{\partial^2\phi}{\partial s_{01}\partial s_{11}}\frac{\sqrt{3}}{4}\frac{\partial^2\phi}{\partial s_{02}\partial s_{12}}.\end{aligned} \tag{14}$$

Going along the same lines, the general method to extract second derivative in rotated coordinate system is given by

$$\frac{\partial^2\phi}{\partial s_{0i}\partial s_{2j}} = \frac{\partial}{\partial s_{0i}}\frac{\partial\phi}{\partial s_{2j}} = \frac{\partial s_{0i'}}{\partial s_{0i}}\frac{\partial}{\partial s_{02'}}\left(\frac{\partial\phi}{\partial s_{2j}}\right) + \frac{\partial s_{0\text{other}'}}{\partial s_{0i}}\frac{\partial}{\partial s_{0\text{other}'}}\left(\frac{\partial\phi}{\partial s_{2j}}\right)$$
$$= \sum_{i'=1}^{2}\frac{\partial s_{0i'}}{\partial s_{0i}}\frac{\partial}{\partial s_{0i'}}\left(\frac{\partial\phi}{\partial s_{2j}}\right) = \sum_{i'=1}^{2}\frac{\partial s_{i'}}{\partial s_i}\frac{\partial}{\partial s_{0i'}}\sum_{j'=1}^{2}\frac{\partial s_{2j'}}{\partial s_{2j}}\left(\frac{\partial\phi}{\partial s_{2j'}}\right)$$
$$= \sum_{i'=1}^{2}\sum_{j'=1}^{2}\left(\frac{\partial s_{i'}}{\partial s_i}\right)\left(\frac{\partial s_{j'}}{\partial s_j}\right)\left(\frac{\partial^2\phi}{\partial s_{01'}\partial s_{2j'}}\right). \tag{15}$$

Since there are only ϕ_{01}^{11} and ϕ_{02}^{12} as non-vanishing array ϕ_{0i}^{1j} elements, we have

$$\phi_{01}^{21} = \frac{\partial x'}{\partial x}\frac{\partial x'}{\partial x}\phi_{01}^{11} + \frac{\partial y'}{\partial x}\frac{\partial y'}{\partial x}\phi_{02}^{12} = \frac{1}{4}\phi_{01}^{11} + \frac{3}{4}\phi_{02}^{12}, \tag{16}$$

$$\phi_{01}^{21} = \frac{1}{4}\phi_{01}^{11} + \frac{3}{4}\phi_{02}^{12}, \tag{17}$$

$$\phi_{01}^{22} = \frac{\sqrt{3}}{4}\phi_{01}^{11} - \frac{\sqrt{3}}{4}\phi_{02}^{12}, \tag{18}$$

$$\phi_{02}^{21} = \frac{\sqrt{3}}{4}\phi_{01}^{11} - \frac{\sqrt{3}}{4}\phi_{02}^{12}, \tag{19}$$

$$\phi_{02}^{22} = -\frac{3}{4}\phi_{01}^{11} + \frac{1}{4}\phi_{02}^{12}. \tag{20}$$

For site 3, we rotate x and y by -120° and

$$x' = -\frac{x}{2} + \frac{\sqrt{3}}{2}y, \tag{21}$$

$$y' = -\frac{\sqrt{3}}{2}x - \frac{y}{2}. \tag{22}$$

In the same manner we get the other equations by replacing 2 by 3.

Appendix III. Force constants for graphene

$$\phi_{011}^{011} = \phi_{012}^{012} = \phi_{021}^{021} = \phi_{022}^{022} = 151.312\ \text{eV/Å}^{-2}, \tag{23}$$

$$\phi_{012}^{022} = -65.322\ \text{eV/Å}^{-2}, \tag{24}$$

$$\phi_{011}^{021} = \phi_{021}^{011} = -41.654 \text{ eV/Å}^{-2}, \tag{25}$$

$$\phi_{011}^{111} = \phi_{011}^{311} = \phi_{011}^{411} = \phi_{011}^{611} = -1.498 \text{ eV/Å}^{-2}, \tag{26}$$

$$\phi_{021}^{011} = \phi_{011}^{012} = \phi_{021}^{012} = \phi_{022}^{011} = 0, \tag{27}$$

$$\phi_{012}^{311} = \phi_{011}^{612} = -0.865 \text{ eV/Å}^{-2}, \tag{28}$$

$$\phi_{011}^{112} = \phi_{012}^{412} = 0.865 \text{ eV/Å}^{-2}, \tag{29}$$

$$\phi_{012}^{611} = \phi_{011}^{312} = 11.334 \text{ eV/Å}^{-2}, \tag{30}$$

$$\phi_{012}^{111} = \phi_{011}^{412} = -11.334 \text{ eV/Å}^{-2}, \tag{31}$$

$$\phi_{012}^{112} = \phi_{012}^{312} = \phi_{012}^{412} = \phi_{012}^{612} = 4.547 \text{ eV/Å}^{-2}, \tag{32}$$

$$\phi_{011}^{211} = \phi_{011}^{511} = 7.569 \text{ eV/Å}^{-2}, \tag{33}$$

$$\phi_{011}^{212} = \phi_{012}^{511} = -6.099 \text{ eV/Å}^{-2}, \tag{34}$$

$$\phi_{011}^{512} = \phi_{012}^{211} = 6.099 \text{ eV/Å}^{-2}, \tag{35}$$

$$\phi_{012}^{212} = \phi_{012}^{512} = -4.520 \text{ eV/Å}^{-2}, \tag{36}$$

$$\phi_{011}^{321} = \phi_{011}^{421} = -59.405 \text{ eV/Å}^{-2}, \tag{37}$$

$$\phi_{011}^{322} = \phi_{012}^{321} = -10.249 \text{ eV/Å}^{-2}, \tag{38}$$

$$\phi_{011}^{422} = \phi_{012}^{421} = 10.249 \text{ eV/Å}^{-2}, \tag{39}$$

$$\phi_{012}^{322} = \phi_{012}^{422} = -47.571 \text{ eV/Å}^{-2}. \tag{40}$$

We have calculated the force constants along z-direction also but the values are comparatively lower than the force constants along x-direction and y-direction.

$$\phi_{013}^{013} = \phi_{023}^{023} = 11.596 \text{ eV/Å}^{-2}, \tag{41}$$

$$\phi_{013}^{023} = \phi_{013}^{323} = \phi_{013}^{423} = -6.409 \text{ eV/Å}^{-2}, \tag{42}$$

$$\phi_{013}^{113} = \phi_{013}^{213} = \phi_{013}^{313} = \phi_{013}^{413} = \phi_{013}^{513} = \phi_{013}^{613} = \phi_{013}^{423} = 1.272 \text{ eV/Å}^{-2}. \tag{43}$$

References

[1] J De Launay, *Solid State Phys.* **3**, 203 (1957)
[2] R Nicklow, W Wakabayashi and H G Smith, *Phys. Rev. B* **5**, 4951 (1972)
[3] A A Ahmadieh and H A Rafizadeh, *Phys. Rev. B* **7**, 4527 (1973)
[4] A P P Nicholson and D J Bacon, *J. Phys. C* **10**, 2295 (1977)
[5] M Maeda, Y Kuramoto and C Horie, *J. Phys. Soc. Jpn. Lett.* **47**, 337 (1979)
[6] R Al-Jishi and G Dresselhaus, *Phys. Rev. B* **26**, 4514 (1982)
[7] H Gupta, J Malhotra, N Rani and B Tripathi, *Phys. Rev. B* **33**, 7285 (1986)
[8] L Lang, S Doyen-Lang, A Charlier and M F Charlier, *Phys. Rev. B* **49**, 5672 (1994)
[9] J Maultzsch, S Reich, C Thomsen, H Reequardt and P Ordejon, *Phys. Rev. Lett.* **92**, 075501 (2004)
[10] M Mohr, J Maultzsch, E Dobardzic, I Milosevic, M Damnjanovic, A Bosak, M Krish and C Thomsen, *Phys. Rev. B* **76**, 035439 (2007)
[11] D Sánchez-Portal, E Artacho and J M Soler, *Phys. Rev. B* **59**, 12678 (1999)
[12] O Dubay and G Kresse, *Phys. Rev. B* **67**, 035401 (2003)
[13] A Charlier, E McRae, M-F Charlier, A Spire and S Forster, *Phys. Rev. B* **57**, 6689 (1998)
[14] A Gruneis, R Saito, T Kimura, L G Cancado, M A Primenta, A Jorio, A G Souza Filho, G Dresselhaus and M S Dresselhaus, *Phys. Rev. B* **65**, 155405 (2002)
[15] C Mapelli, C Castiglioni and G Zerbi, *Phys. Rev. B* **60**, 12710 (1999)
[16] V N Popov and P Lambin, *Phys. Rev. B* **73**, 085407 (2006)
[17] N Mounet and N Marzari, *Phys. Rev. B* **71**, 205214 (2005)
[18] D W Brenner, O A Shenderova, J A Harrison, S J Stuart, B Ni and S B Sinnott, *J. Phys.: Condens. Matter* **14**, 783 (2002)
[19] D Goldberg, Y Bando, L Bourgeois, K Kurashima and T Sato, *Appl. Phys. Lett.* **77**, 13 (2000)
[20] R Ma, Y Bando and T Sato, *Adv. Mater.* **14**, 366 (2002)
[21] D Kumar, V Verma, H S Bhatti and K Dharamvir, *J. Nanomater.* 2011, Article ID 127952, 6 pages, 2011, DOI: 10.1155/2011/127952
[22] D Kumar, V Verma and K Dharamvir, *J. Nano Res.* **15**, 1 (2011)
[23] D Kumar, V Verma, K Dharamvir and H S Bhatti, *AIP Proceedings* **1393**, 207 (2011)
[24] S Reich, A C Ferrari, R Arenal, A Loiseau, I Bello and J Robertson, *Phys. Rev. B* **71**, 205201 (2005)
[25] J Q Lu, T E Kopley, N Moll, D Roitman, D Chamberlin, Q Fu, J Liu, T P Russell, D A Rider, I Manners and M A Winnik, *Chem. Mater.* **17**, 2227 (2005)
[26] P Saxena and S P Sanyal, *Pramana – J. Phys.* **67**, 305 (2006)
[27] V N Popov, V E Van Doren and M Balkanski, *Phys. Rev. B* **59**, 8355 (1999)